Formation Accelerated Stress Test (FAST): A New Technique to Study Anode Passivation in Lithium-ion Cells using Differential Capacity, Low Salt Concentration and Low Temperature.

Roby Gauthier[a], Hongyi Lin[a,c], Haotian Chen[e], Venkatsubramanian Viswanathan[a,c,d], Jay Whitacre[b*]

[a]Department of Mechanical Engineering, Carnegie Mellon University, Pittsburgh 15213, USA

[b]Department of Material Science, Carnegie Mellon University, Pittsburgh 15213, USA

[c]Department of Mechanical Engineering, University of Michigan, Ann Arbor, Michigan 48109, USA.

[d]Department of Aerospace Engineering, University of Michigan, Ann Arbor, Michigan 48109, USA.

[e]Michigan Institute for Data & AI in Society, University of Michigan, Ann Arbor, Michigan 48109, USA.

*whitacre@andrew.cmu.edu

Abstract

This study investigates the formation and properties of the solid electrolyte interface (SEI) in lithium-ion batteries under varying salt concentrations (0.4M, 0.8M, 1.2M) and low formation temperatures. This method was used as a formation accelerated stress

test (FAST) to evaluate the impact of different solvent blends and additives on anode passivation using the reduction rate of ethyl methyl carbonate (EMC) seen in the differential capacity of cells containing them as a performance metric. Electrolytes containing a mixture of vinylene carbonate and ethylene sulfate showed superior passivation, while a 3:7 mixture of fluoroethylene carbonate and ethyl methyl carbonate proved to be the most effective at passivating. Furthermore, the low-viscosity solvents methyl acetate and acetonitrile significantly enhanced SEI passivation during formation at the anode due to lower graphite exfoliation. We also show that the differential capacity data correlate with long-term cycling performance for some of the chemistry studied here. These results provide valuable insights for the efficient design of a new formation accelerated stress test (FAST) that could accelerate the discovery of high-performance electrolytes through rapid monitoring of SEI passivation during formation.

Introduction

In recent years, the lithium-ion battery sector has experienced rapid growth, mainly due to its important role as a source of energy storage for electric vehicles, portable electronics, and the grid. This surge in demand is evident in the market's exponential expansion, which went from a ~ 1 GWh annual market size in 2000 to an impressive 0.8 TWh in 2021.[1,2] However, despite such advancements, fully grasping the complexities of the solid electrolyte interface (SEI), a key component of lithium-ion batteries, remains

challenging. A particularly challenging aspect is the prediction of the exact composition, structure, and passivation-related properties of the SEI based on the nature of the electrolyte, the cycling protocol, and other cell properties. This gap in knowledge presents a significant barrier to determining how specific SEI and electrolyte characteristics quantitatively influence the overall lifespan and efficiency of the battery cell.

However, it is well-established that certain additives, such as vinylene carbonate (VC), ethylene sulfate (DTD), fluoroethylene carbonate (FEC), and lithium difluoro(oxalato)borate (LiDFOB) can improve the performance and lifetime of lithium-ion and/or lithium metal batteries.[3–8] The performance improvement offered by those additives could possibly be the result of the passivation of the anode surface by polymers or inorganic species such as polyvinylene carbonate, lithium fluoride, lithium oxalate, and lithium sulfate, among others.[8–10]

In the past, experimental methods related to transport (e.g., electrochemical impedance spectroscopy, ion conductivity), morphology (e.g., CT-scan, jelly roll thickness), gas volume (e.g., Archimedes' principle), and open circuit voltage storage measurements, among other techniques, were used to predict and monitor cell performance.[11–20] However, further development is required to fully grasp the complexity of the SEI, which is also related to cell lifetime.

Recent studies used characterization techniques such as Nuclear Magnetic Resonance (NMR), X-ray Photoelectron Spectroscopy (XPS), and Transmission Electron Microscopy (TEM), as well as modeling to better understand the complex chemistry and

physics occurring at the electrode interfaces under specific conditions.[21–26] Ethylene carbonate (EC) based electrolytes have been studied significantly in that regard. It is generally accepted that EC reduces following two main reaction pathways, among other possible pathways.[22,27–31] A first possible single electron pathway, which forms lithium alkyl carbonates, such as lithium ethylene dicarbonate (LEDC), and a second two-electron pathway, which forms lithium carbonate:

$$2\ EC + 2\ Li^+ + 2\ e^- \rightarrow LEDC + C_2H_4 \qquad (1)$$

$$EC + 2\ Li^+ + 2\ e^- \rightarrow Li_2CO_3 + C_2H_4 \qquad (2)$$

Lithium ethylene dicarbonate can then react in the presence of water to form lithium ethylene monocarbonate (LEMC) via ethylene glycol as an intermediate, while lithium carbonate can react with $LiPF_6$ to form LiF.[30,32,33] Both thermodynamically and kinetically, equation (1) appears to be preferred over equation (2) at low relative salt concentrations at the anode interface. This preference arises from the change in Li^+/EC stoichiometry. The dependence of the SEI composition on salt concentration has been observed before using X-ray photoelectron spectroscopy (XPS), Energy Dispersive X-ray Spectrometry (EDX) and Nuclear Magnetic Resonance Spectroscopy (NMR) in cells with graphite anodes containing $LiPF_6$ and propylene carbonate (PC), where higher salt concentrations resulted in a solid electrolyte interphase (SEI) richer in LiF and poorer in lithium propylene dicarbonate (LPDC) compared to lower salt concentrations.[34] Furthermore, in lithium-ion cells containing lithium bis(trifluoromethanesulfonyl)imide (LiTFSI) as a salt and dimethyl sulfoxide (DMSO) as a solvent, high salt concentrations (>2.5 M) created a passivating SEI, while low salt concentrations (1 M) resulted in

solvent intercalation into graphite.[35] Similar findings were observed for other cell chemistries.[36–38]

In addition to the impact of salt concentration on SEI performance, temperature also has an influence. For example, Transmission Electron Microscopy (TEM) measurements revealed that the thickness of the SEI increases with higher cycling temperatures, while cross-sectional SEM indicated that elevated temperatures result in a more uniform SEI.[39,40] Additionally, using XPS and FTIR, researchers observed that SEI formation on graphite at 60°C produced lithium carbonate-rich SEI when the electrolyte consisted of 1 M LiClO4 EC:DME 1:1. In contrast, formation at 25°C for the same chemistry, resulted in a lithium carbonate-poor SEI and graphite delamination, which resulted in poor cycling performance.[40]

Building on previous research that demonstrated the effectiveness of low salt concentration as a method for accelerated stress testing, we decided to study the formation of different electrolyte formulations at different salt concentrations and formation temperatures. Then, we compared some of those findings with their long-term cycling performance.[41] Since the SEI is less passivating under low salt concentration and low temperature, those conditions can be used to better understand how different solvents and additives influence passivation. Additionally, low salt concentration helps isolate the effects of the solvent and additives on SEI passivation from those of the salt. Furthermore, the results from the present study could potentially be relevant to very fast charging applications under low-temperature conditions where large salt concentration gradients develop.[42] Finally, we aim to gain new insights that could assist researchers in accelerating electrolyte discovery.

Methods

Pouch cells

402035-size pouch cells without electrolyte were received from Li-Fun Technology (Zhuzhou, Hunan, China) with polycrystalline $Li(Ni_{0.6}Mn_{0.2}Co_{0.2})O_2$ (NMC622) as the positive electrode and artificial graphite as the negative electrode. The cell was balanced to 4.5 V (the threshold voltage for lithium plating during the first charge, determined by the cathode and anode mass loading). The first charge capacity of the cells was ~250 mAh at 4.3 V. Prior to being filled with electrolyte, each cell was cut below the seal and dried in a vacuum oven at 80°C for a minimum of 12 hours. The thicknesses, mass loading, and active area of each electrode can be found in Table S5.

Electrolyte preparation

All electrolytes contained ethylene carbonate (EC; GELON, 99.9%, <20 ppm water) mixed with linear carbonates, an ester or a nitrile such as ethyl methyl carbonate (EMC; GELON, 99.9%, <20 ppm water), dimethyl carbonate (DMC; GELON, 99.9%), methyl acetate (MA; GELON, 99.9%), acetonitrile (ACN; Sigma-Aldrich, >99.8%), propionitrile (PN; Tokyo chemical industry (TCI), >98%) or valeronitrile (VN; Tokyo chemical industry (TCI), >98%). Lithium hexafluorophosphate ($LiPF_6$; GELON, 99.9%, <20 ppm water) was added to the main mixture in various concentrations of 0.4 M, 0.8 M or 1.2 M. Vinylene carbonate (VC; BASF, 99.5%, <100 ppm water), ethylene sulfate (DTD; Tinci Materials, ≥98%), fluoroethylene carbonate (FEC; GELON, 99.9%) and/or lithium

difluoro(oxalato)borate (LiDFOB; GELON, 99.9%) were added as additives when needed. Tables 1 and 2 show the different electrolyte compositions used in this work with their respective formation and cycling conditions.

The pouch cells were filled with 0.8 mL of electrolyte in an argon-filled glove box and then heat sealed at a temperature of ~160°C.

Formation

After cells were filled with electrolyte, they were kept at 1.5 V for 24 hours for the purpose of wetting the jelly roll and then charged at a constant current of C/20 to their maximum voltage, and then they were kept at a constant voltage until the current decreased to C/40. However, cells containing LiDFOB skipped the 24-hour wetting step at 1.5 V in order to prevent any LiDFOB reduction before the differential capacity measurement.[43] If the cell underwent cycling, the cell was charged at C/20 to a maximum voltage of 4.3 V and then discharged at a constant current of C/20 to 3.8 V. Cells were then degassed in a glovebox before they were connected back to the Neware for long-term cycling. The cell temperatures were kept at 20°C, 30°C, or 40°C during the formation process, as specified in Table 1 and the main text.

Table 1: List of electrolytes used in this work and their respective formation conditions for cells that were not subjected to long-term cycling.

$LiPF_6$ molarity	Solvent and Additives (by mass)	Temperature (°C)	C-rate	Wetting (24h at 1.5V)
0.4, 0.8, 1.2 M	EC:EMC 3:7	20, 30 (at 0.4 M), 40	C/20, C/40 (at 20°C and 0.4 M)	Yes
0.4, 0.8, 1.2 M	EC:EMC 3:7 2% VC	20	C/20	Yes
0.4, 0.8, 1.2 M	EC:EMC 3:7 2% VC + 1% DTD	20, 40 (at 1.2 M)	C/20	Yes
0.4, 0.8, 1.2 M	EC:EMC 3:7 1% DTD	20	C/20	Yes
0.4 M	EC:EMC 3:7 2% LiDFOB	20	C/20	No
0.4 M	FEC:EMC 3:7, EC:DMC 3:7, EC:EMC 1:9	20	C/20	Yes
0.4 M	EC:EMC 3:7 + 30% MA	20	C/20	Yes
0.4 M	EC:EMC:MA 3:4:3, EC:EMC:ACN 3:4:3, EC:EMC:PN 3:4:3, EC:EMC:VN 3:4:3	20	C/20	Yes

Long-term cycling

After the cells were formed at 40°C and C/20, cells were degassed in a glovebox before they were connected back to the Neware for long-term cycling. Cycling was performed at 55°C and C/2, with C/10 checkup cycles every 50 cycles. Cycling was performed for 1100 cycles, and the ΔV value was calculated using the difference between the average charge and discharge voltage for each cycle number. The electrolytes tested during long-term cycling were 1.2 M LiPF6 EC:EMC 3:7, 1.2 M LiPF6 FEC:EMC 3:7 and 1.2 M LiPF6 EC:EMC 3:7 2% VC + 1% DTD (ratio and percentage by mass).

Density functional theory calculations

Density functional theory calculations were performed using the Gaussian 16 software.[44] Calculations were performed using the B3LYP functional at the 6-311++G(2df,2dp) level using the IEFPCM polarizable continuum model with a relative permittivity of 20.[45–49] All structures were optimized from an initial guess, and a frequency calculation was performed. This was done in order to calculate the Gibbs free energy of formation of each structure at 298 K and to also verify that no imaginary frequencies were present. The reduction potential of each molecule was then calculated following the method used previously by Self et al.[50]

Thickness measurements

Thickness measurements were acquired on two equivalent cells using either a micrometer (iGaging, California, USA) for cells containing nitriles or a digital caliper (Mitutoyo, Illinois, USA) for all other cells. All measurements were acquired in the center of the jelly roll of the pouch cells. Cells were degassed prior to any measurement to eliminate the thickness increase due to gas production. The micrometer measurements were performed using a constant applied pressure for all cells by halting after the first audible click. In contrast, digital caliper measurements were collected when the surface of the cells was judged to be flat. The variation between two measurements on the same cell averaged 60 microns for micrometer measurements, while the maximum variation between two measurements on the same cell using the digital caliper was 50 microns.

Results and Discussions

Motivated by past research indicating that low salt concentrations can accelerate lithium-ion cell failure and driven by the need to accelerate electrolyte discoveries, we undertook cycling of lithium-ion pouch cells with low salt concentrations.[41,51] Interestingly, we then observed a significant reduction of EMC at an offset voltage of 3.1 V when NMC622/graphite cells filled with 0.4 M $LiPF_6$ EC:EMC 3:7 were formed at 20°C,[52,53] while this was not observed to occur at 40°C. Figure 1. a) presents this data, revealing a non-linear relationship between the rate of EMC reduction at 3.1 V and the formation temperature. By integrating the dQ/dV curve between 3.1 and 3.4 V and assuming negligible EMC reduction at 40°C (see Figure S1), it is estimated that approximately 26 mAh of lithium-ion are consumed due to EMC reduction at 20°C, compared to 5 mAh at 30°C. In addition, it is clear that increasing the formation temperature gradually results in better passivation against EMC reduction and causes a shift in the EC reduction potential toward lower full-cell voltage.

To better understand the kinetics behind the phenomenon, cells with the same chemistry were formed at two different C-rates, C/20 and C/40, and a temperature of 20°C. Figure 1. b) shows this data. Interestingly, varying C-rates don't appear to change the EMC reduction rate significantly under the conditions studied here, indicating that it is unlikely that low electrolyte conductivity is the cause behind this phenomenon.

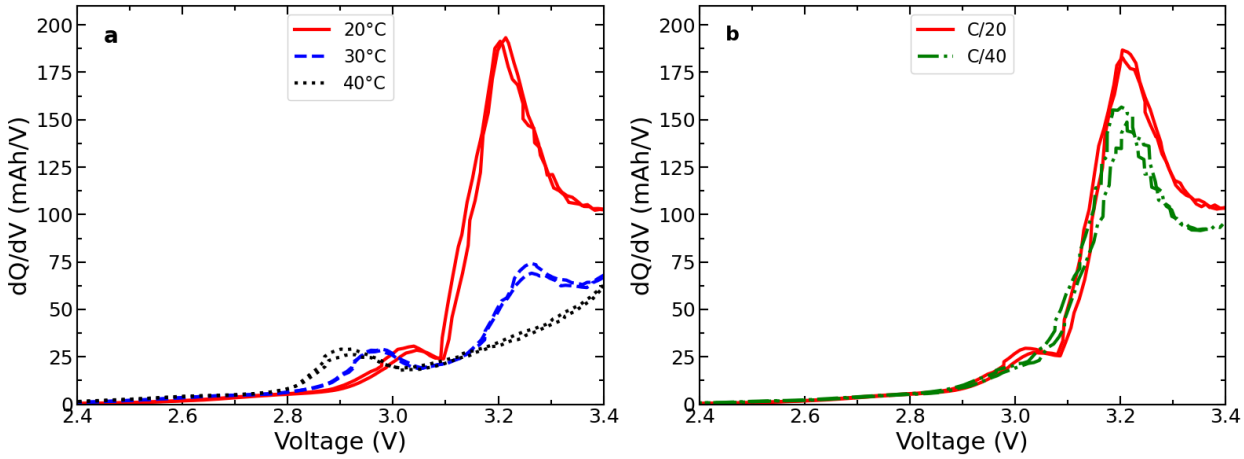

Figure 1: Differential capacity versus voltage plots that were obtained by performing cell formations at a) three different temperatures or b) two different C-rate, as indicated in the legend, for electrolytes containing 0.4 M $LiPF_6$ EC:EMC 3:7. Charging was done at a constant C-rate of C/20 for subfigure a) and a C-rate of C/20 or C/40 and a temperature of 20°C for subfigure b).

To better understand how the salt concentration affects this phenomenon, cells with different salt concentrations were made and tested. Figure 2a) shows that when salt concentration was increased from 0.4 M to 1.2 M, the rate of EMC reduction was observed to decrease. In contrast, Figure 2. b) shows that the impact of salt concentration has no influence on EMC reduction at a formation temperature of 40°C. This effect was also observed in lithium iron phosphate (LFP)/graphite full cells at a normal salt concentration (1.2 M) and at a temperature of 20°C by Zhang et al., who showed that exfoliation of the graphite occurred under those conditions using X-ray diffraction.[54] While Zhang et al. were motivated to prevent graphite exfoliation from

occurring by optimizing the electrolyte, here we take advantage of this EMC reduction effect to study the degree of passivation of the solid electrolyte interface (SEI) for different electrolyte formulations.

We reason that cell performance at the anode, when the salt chemistry is fixed, should mostly result from electrically insulting passivation of the anode by the solvent and low linear carbonate reduction. Linear carbonate reduction is known to produce lithium alkoxides, which results in the degradation of the electrolyte via transesterification and could result in a loss of performance.[55] Additionally, poor passivation that is not electrically insulting can cause continuous SEI growth, resulting in lithium inventory loss and impedance growth. In line with this reasoning, we looked at the effect of adding additives to the electrolyte. Zhang et al. showed that adding 2% VC to an electrolyte containing 1.2 M $LiPF_6$ EC:EMC 3:7 was enough to passivate the graphite against the reduction of EMC and enough to stop the resulting graphite exfoliation. Figure 2. c) shows the effect of adding 2% VC + 1% DTD to cells containing electrolytes with different salt concentrations when those cells are formed at 20°C. It is observed that slight EMC reduction occurs when the salt concentration is 0.8 M; however, this reduction doesn't occur at concentrations of 1.2 M, and very little EMC reduction occurs at 0.4 M, showing that EMC reduction follows a non-monotonic relationship versus salt concentration for this electrolyte, which could be the result of the coupling of two competing effects.

Figure 2. d) shows that EMC reduction doesn’t occur at a formation temperature of 40°C when the salt concentration is 1.2 M in a cell containing those additives. Figure 2. d)

also shows that formation at 20°C results in full cell reduction potentials 0.1 V higher than those at 40°C for EC (2.9 V), DTD (2.5 V), and VC (2.8 V).

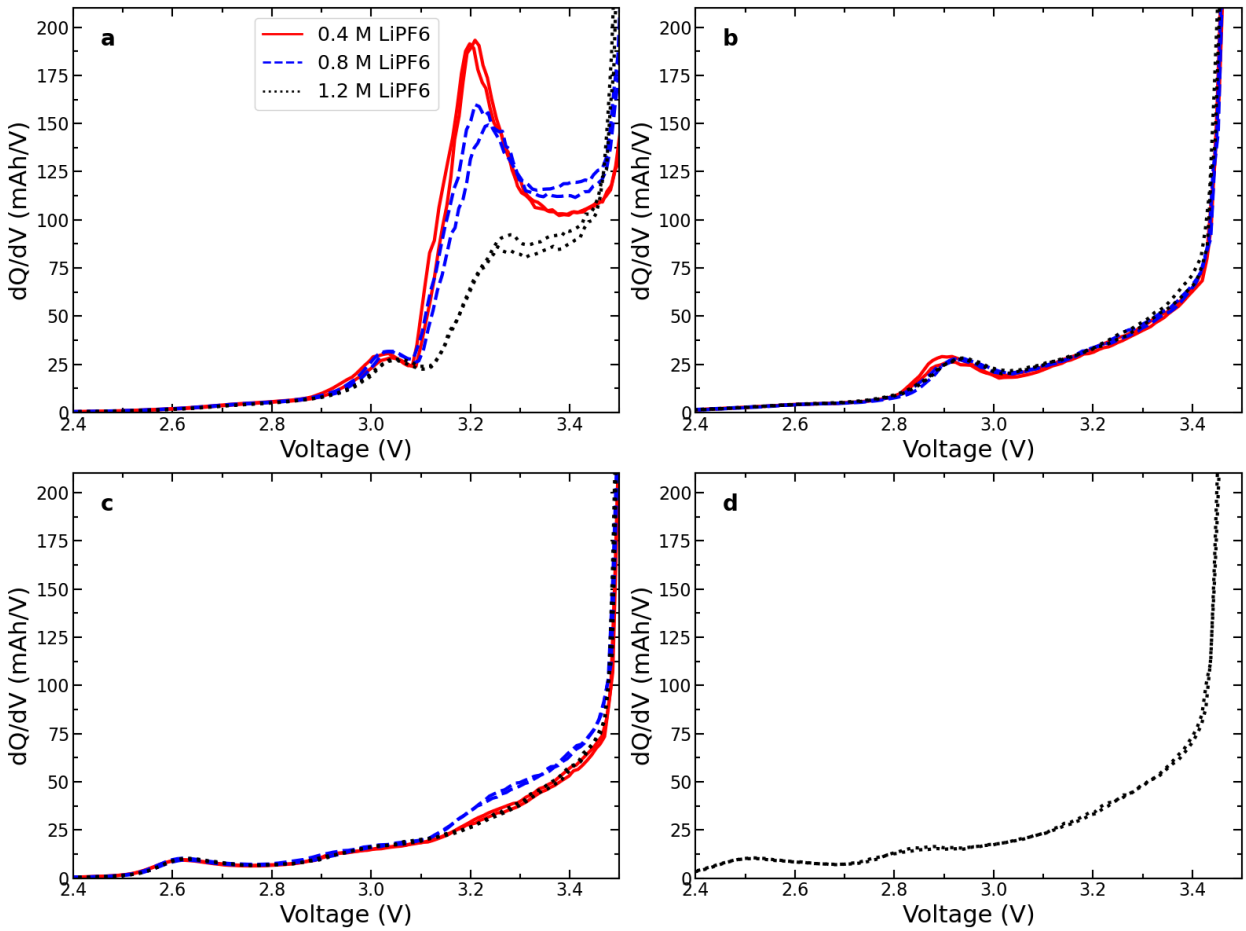

Figure 2: Differential capacity versus full cell voltage for cells formed at a), c) 20°C and b), d) 40°C. Subfigures a) and b) show data for electrolytes containing the baseline solvent (EC:EMC 3:7), while subfigures c) and d) also include the additive blend 2% VC + 1% DTD in addition to the baseline solvent. Different line styles and colors are used to represent the different salt concentrations (0.4 M $LiPF_6$ for solid red, 0.8 M $LiPF_6$ for dashed blue, and 1.2 M $LiPF_6$ for dotted black). All experiments were performed at a constant current of C/20 after wetting until their maximum voltages.

To understand the reason behind the non-linearity in the EMC reduction rate at 20°C for cells containing 2% VC + 1% DTD, similar experiments were performed for cells containing only 2% VC or only 1% DTD as added additives. The results of these experiments performed at 20°C are shown in Figure 3. a) for 2% VC and 2. b) for 1% DTD. Figure 3. a) and b) shows that while the two additives have similar EMC reduction rates at a salt concentration of 1.2 M, the electrolyte containing 2% VC is more sensitive to a decrease in salt concentration than 1% DTD when it comes to passivation against EMC reduction. Figure 3. a) shows nonlinearity for the EMC reduction rate as a function of salt concentration for VC-containing electrolytes, while the EMC reduction rate is almost constant as a function of salt concentration in Figure 3. b) for DTD-containing electrolytes. This suggests that vinylene carbonate could be the reason behind the nonlinearity as a function of salt concentration shown in Figure 2. c) for 2% VC + 1% DTD-based electrolytes. We hypothesize that passivation improves at high salt concentrations due to an increase in inorganic components in the SEI. In contrast, the increase in passivation at low salt concentration could possibly result from the change of Li^+/VC stoichiometry at the interface, resulting in longer polyvinyl carbonate chains. However, fully understanding that nonlinearity is beyond the scope of the current work and more research is needed to confirm that hypothesis.

In order to elucidate the different sensitivities to salt concentrations for different electrolytes during reduction, Density Functional Theory (DFT) calculations using the

B3LYP functional and the IEFPCM solvent model at the 6-311++G(2df,2pd) level were performed. The rationale for these DFT calculations is that, in a low salt concentration electrolyte, a smaller percentage of solvent is present in the solvation shells, leaving more of it free in the electrolyte. If the free solvent molecules are still able to reduce easily, even without the presence of a lithium-ion, then the passivation of graphite by these molecules should be insensitive to the amount of salt in the electrolyte.

In parallel, the accuracy of the functional and basis set used in this work is supported by previous studies showing good agreements of calculated reduction potentials with experiments. Tables S1 and S2 also show good agreement (~0.3-0.4 eV) with experimental ionization energy and electron affinity for a multitude of molecules, supporting its accuracy for the present work. [53,56,57]

Table 2 shows that the reduction potentials of ethylene carbonate and vinylene carbonate change upon the presence of a lithium-ion, with ethylene carbonate shifting from -0.51 V vs. Li/Li^+ to 0.4 V vs. Li/Li^+ and vinylene carbonate from 0.3 V vs. Li/Li^+ to 0.65 V vs. Li/Li^+ upon lithiation. In contrast, ethylene sulfate shows minimal change upon lithiation, with reduction potentials of 1.74 V vs. Li/Li^+ and 1.89 V vs. Li/Li^+ for the non-lithiated and lithiated states, respectively. This suggests that lithium ions stabilize the reduced states of ethylene carbonate and vinylene carbonate, while ethylene sulfate doesn't need to be stabilized by the ion to reduce. Consequently, ethylene carbonate is unable to reduce in a low salt environment, vinylene carbonate reduction is slowed, and ethylene sulfate reduction is almost unaffected. This is consistent with the results shown in Figures 1a, 2a, and 2b. While this is an interesting hypothesis, alternative

mechanisms could also explain these results. The optimized geometries related to these calculations can be found in Figure S5.

Table 2: Reductions potentials of lithiated and non-lithiated ethylene carbonate, vinylene carbonate, and ethylene sulfate.

Molecule of interest	Non-lithiated reduction potentials (V vs. Li/Li+)	Lithiated reduction potentials (V vs. Li/Li+)
Ethylene carbonate	-0.51	0.4
Vinylene carbonate	0.3	0.65
Ethylene sulfate	1.74	1.89

To further test the passivation ability of different electrolytes, further formation experiments were performed at 20°C. Figure 3. c) shows the results of these experiments for electrolytes that contained 0.4 M $LiPF_6$. Low salt concentrations were utilized to more clearly observe the passivation properties of the different additives. Figure 3. c) shows that, with the exception of electrolytes containing LiDFOB or 2% VC + 1% DTD, the rate of EMC reduction is correlated with the reduction potential of the first reduction event in the full cell; however, it is unclear if there is any causality between those two variables.

If the differential capacity is graphed versus time (See Figure S2), it can be observed that the reduction duration of the first molecule in the cell is proportional to the EMC

reduction rate. This might reflect the smaller SEI thickness required to achieve anode passivation for the electrolytes that reduce faster and have a smaller EMC reduction rate. Figure 3. c) also shows, using the amplitude of EMC reduction at 3.1 - 3.3 V as a metric, that electrolytes that contain 2% VC + 1% DTD or FEC:EMC 3:7 are the best passivating electrolytes among the ones tested, while the EC:EMC 3:7 based electrolyte with no additives or with VC are among the worse tested, and this is interestingly consistent with the capacity fade measured during previous long-term cycling studies (see digitized data from those studies in Figure S3 and S4).[4,56–59] The electrolyte with 2% LiDFOB showed a similar effect as the electrolyte containing 1% DTD in terms of EMC reduction rate; however, LiDFOB didn't passivate against EC reduction while DTD did.

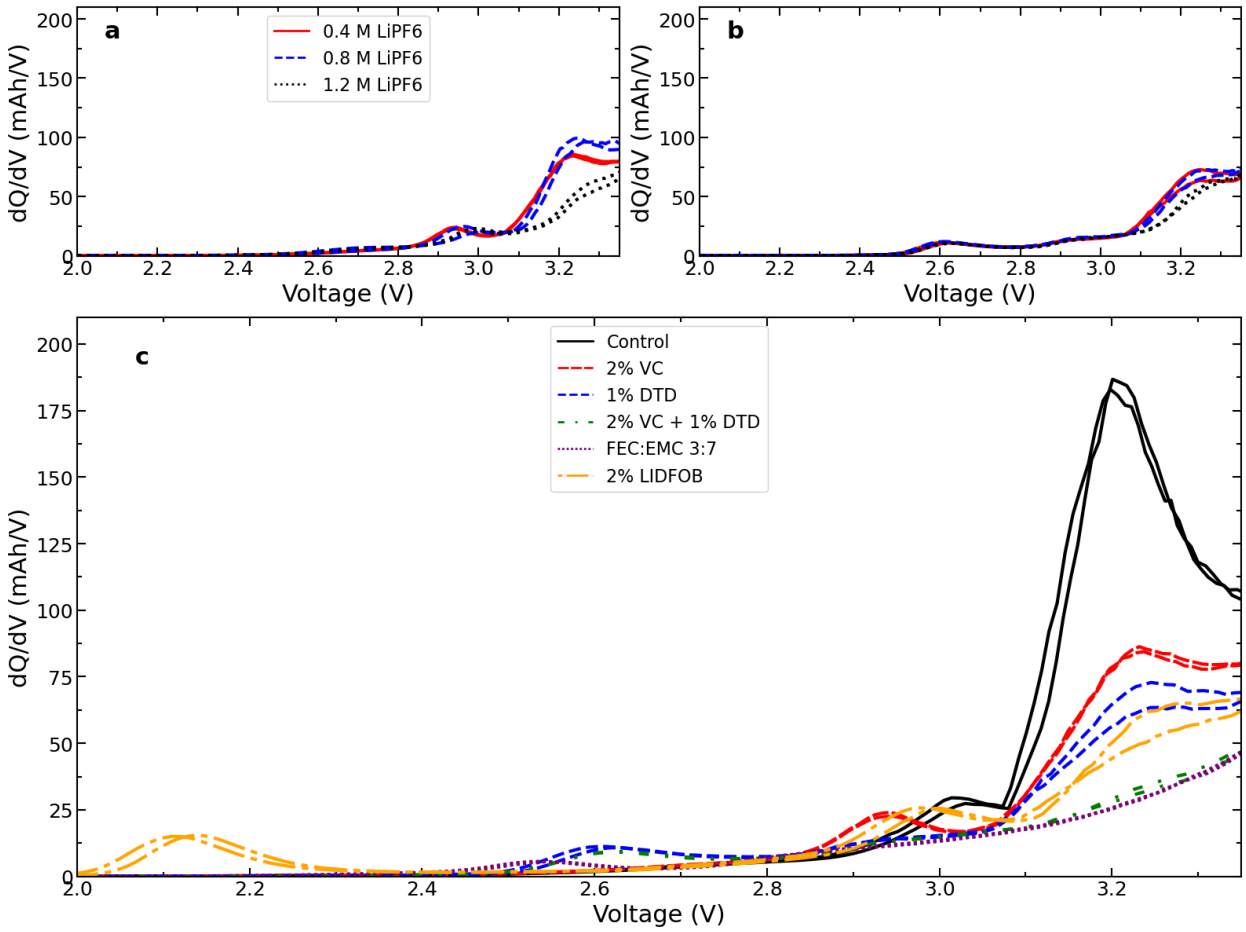

Figure 3: Differential capacity versus voltage plots that were obtained by performing cell formation at 20 °C for different electrolytes. Subfigures a) and b) show the effect of different salt concentrations (0.4 M, 0.8 M, 1.2 M) on EC:EMC 3:7-based electrolytes that contain 2% VC or 1% DTD, respectively. Subfigure c) shows the differential capacity versus voltage that was obtained by performing cell formation at 20°C for different electrolyte formulations and a constant salt concentration of 0.4 M $LiPF_6$. All experiments were performed at a constant current of C/20 after wetting until their maximum voltages, except cells containing LiDFOB, as mentioned in the method section.

Following the study of the effect of different additives on passivation, the effect of different solvent blends on passivation was investigated. Zhang et al. showed that replacing EMC with DMC or decreasing the amount of EC resulted in full graphite passivation in 1.2 M $LiPF_6$-based electrolyte at 20°C.[54] Figure 4a shows that when the salt concentration is low (0.4 M), the DMC-based electrolyte (0.4 M $LiPF_6$ EC:DMC 3:7) no longer passivates against the reduction of the linear carbonate DMC like it was shown to be the case for 1.2 M $LiPF_6$.[54] This is very clear when compared to the very passivating FEC:EMC 3:7 based electrolyte. However, Figure 4b shows that low EC-based electrolytes (0.4 M EC:EMC 1:9) still passivate well at low salt concentrations. It is known that electrolytes that contain less EC are less viscous.[14] As such, it was investigated if low viscosity could be a major contributing factor to passivation. To study this effect, 30% of the EMC in EC:EMC 3:7 was substituted with the low-viscosity solvent methyl acetate (MA).[13,60] Methyl acetate has a viscosity of η = 0.365 cp at 25°C, which is half the viscosity of EMC (η = 0.65 cp at 25°C).[61,62] Figure 4b shows that this substitution results in drastic improvement in the passivation against EMC reduction without decreasing the relative amount of EC in the electrolyte. This result is also observed when the relative amount of EC is not adjusted after the addition of MA (0.4 M $LiPF_6$ EC:EMC 3:7 + 30% MA), as expected. Additionally, DMC has a lower viscosity when compared to EMC (η = 0.59 cp at 25°C for DMC and η = 0.65 cp at 25°C for EMC), and DEC has a larger viscosity (η = 0.75 at 25°C) consistent with the passivation result shown in Figure 4a and the passivation results from Zhang et al.[54]

Advanced Electrolyte Model (AEM) calculations were performed to compare electrolyte properties to the performances shown in Figure 4b. The results are shown in Figure 5. From those calculations, we can observe that reducing the relative amount of EC or substituting some of the EMC with MA decreases the viscosity of the electrolyte, as expected. However, those changes had minimal impact on the transference number, surface tension, and desolvation time. This shows that lithium transport and surface energy of the electrolyte had minimal impact on the anode passivation and the degree of exfoliation of the cells shown here. This suggests that viscosity and stoichiometry (the salt concentrations) have important roles in passivation. Previous research has shown that high-viscosity solvents and those with surface energies similar to graphite (53.6 ± 2.1 mN/m) can facilitate its exfoliation by reducing the shear rate required for the process.[63–66] Graphite exfoliation can then cause SEI cracking, an increase of the active surface area, and more reduction of the electrolyte as a result. In a lithium-ion battery, shear can be caused by lithium intercalation into graphite or gas production, for example. Furthermore, previous research found a correlation between graphite exfoliation, as supported by X-ray diffraction and pressure measurements, and the first cycle coulombic efficiency. Specifically, a cell that contained 1.2 M LiPF6 EC:EMC 3:7 consumed ~ 20 % more lithium than a cell that contained 1.2 M LiPF6 EC:DMC 3:7 during their first cycle, showing a significant impact on SEI growth.

To add more evidence that viscosity plays a role in graphite exfoliation and passivation, three nitriles with increasing viscosity were investigated: Acetonitrile (ACN; η = 0.324 - 0.37 cp at 25°C), Propionitrile (PN; 0.414 cp at 25°C) and Valeronitrile (VN, η = 0.779

cp at 25°C).[61,67] Similar to the case of methyl acetate, each nitrile was mixed with EC:EMC 3:4 to get EC:EMC:X 3:4:3 by mass, where X is a nitrile. Then, $LiPF_6$ was added until a 0.4 M concentration was achieved.

Figure 4c shows the differential capacity of cells containing those three electrolytes and the results are compared to the electrolyte with no nitrile. Interestingly, the reduction peaks with an offset of 3.1 - 3.2 V increase as the number of carbon atoms and the viscosity of the nitrile increases. This peak could be attributed to the reduction of EMC or the nitriles, as both ACN and PN have reduction potentials similar to EMC.[61] Figure 5 also shows AEM calculations for the electrolytes containing ACN or PN. Those calculations further reveal that the overall viscosity of the electrolyte increases as the viscosity of the nitrile rises, while others don't vary significantly, except EC concentration in the solvation shell versus in the bulk. Additional AEM calculations showed that in 0.4 M $LiPF_6$ EC:EMC:ACN 3:4:3, acetonitrile represents 64.4 % of the Li^+ solvation shell by mole, while ethylene carbonate represents only 13.8 %. When ACN is replaced with PN, we get 44.3% PN and 22.1 % EC, while for 0.4 M $LiPF_6$ EC:EMC 3:7 we get 27.4 % EC. This predominance of nitrile in the solvation shell could explain the absence of EC reduction in Figure 4c for the electrolytes containing these nitriles. Despite lower SEI passivation, electrolyte reduction might appear smaller for lower-viscosity electrolytes due to decreased exfoliation.

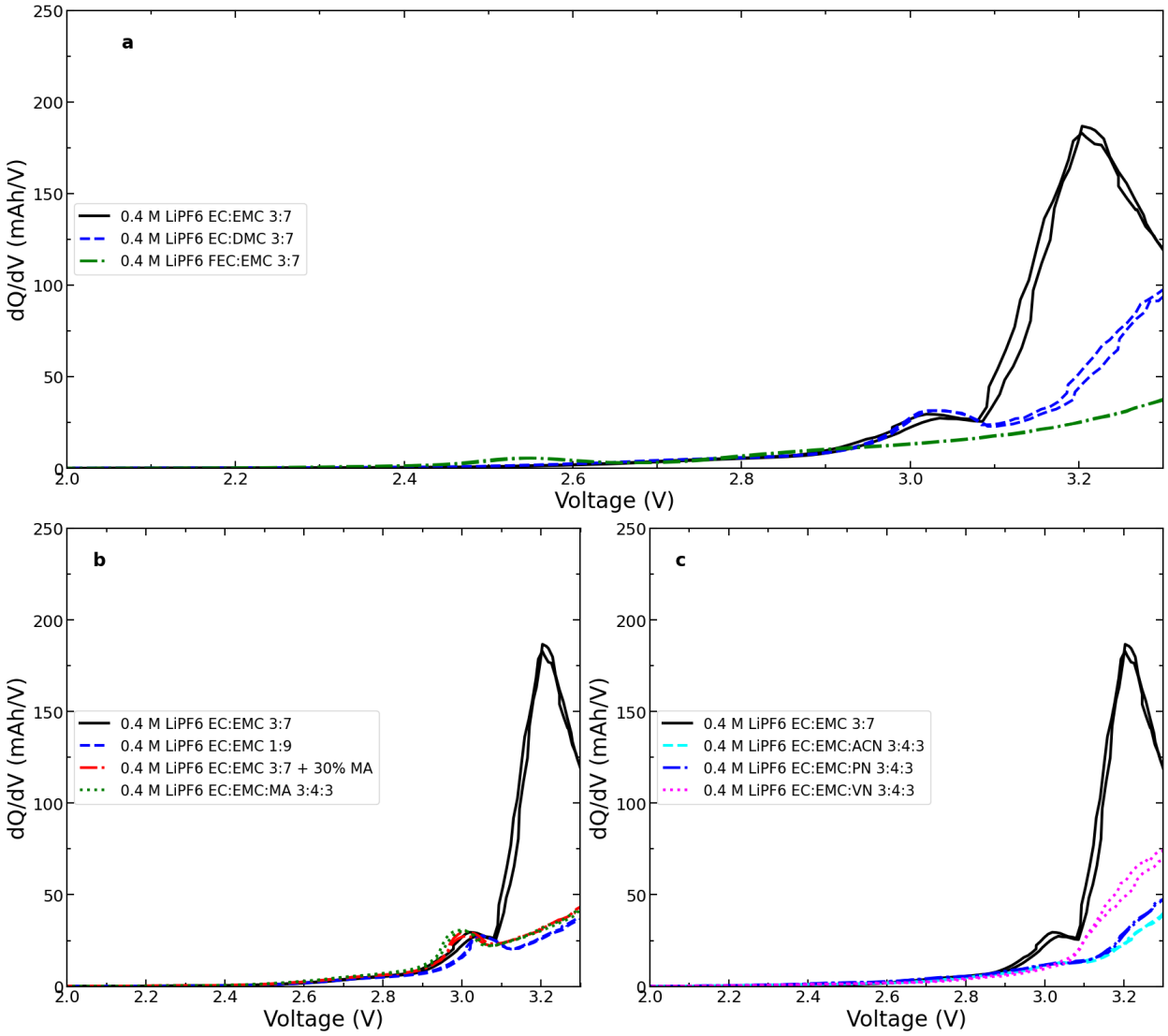

Figure 4: Differential capacity versus voltage plots that were obtained by performing cell formations at 20°C for electrolytes containing different baseline solvents. Charging was done at a constant C-rate of C/20. The corresponding electrolyte formulations are indicated in the legend.

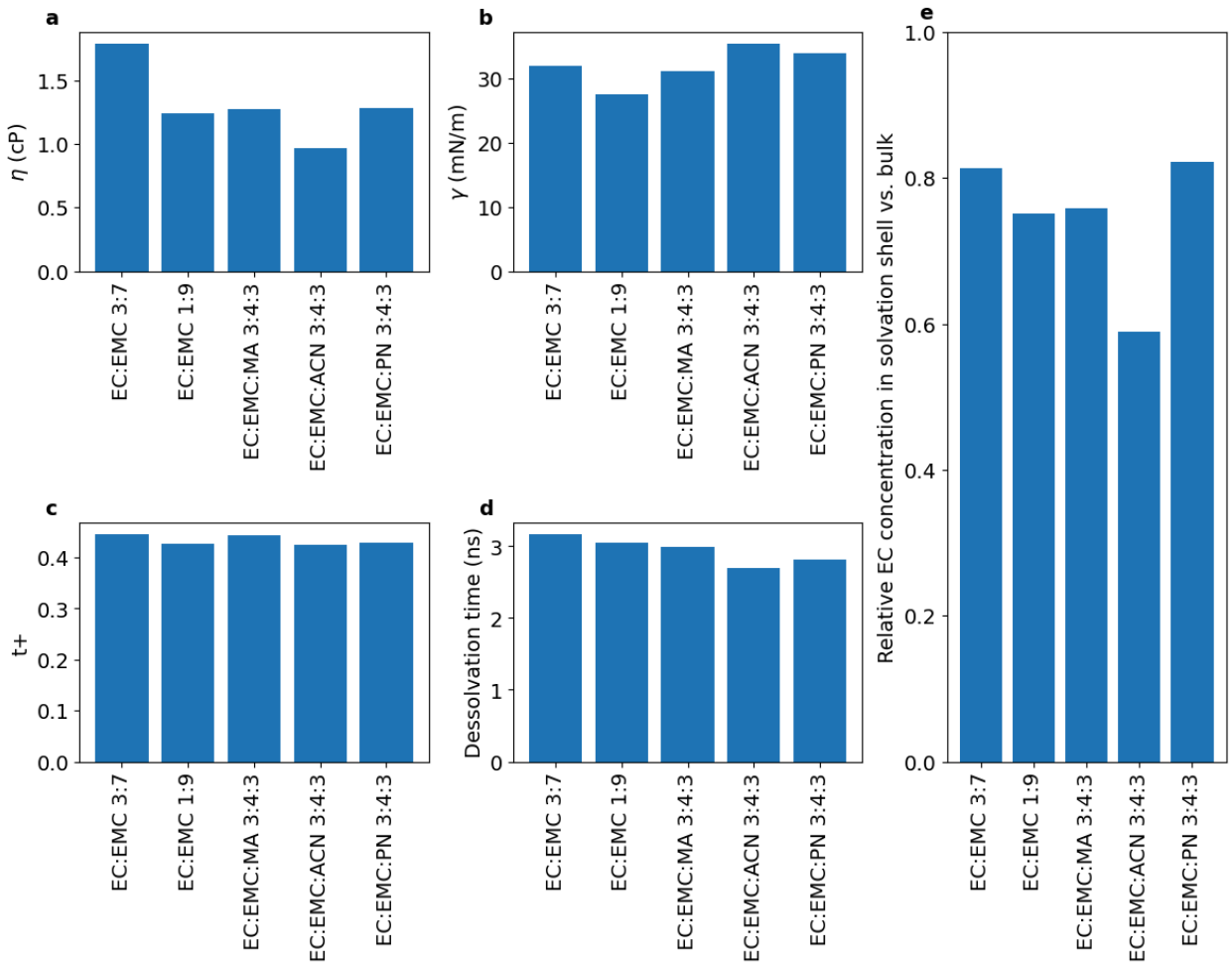

Figure 5: a) Viscosity (η), b) surface tension (γ), c) lithium-ion transport number (t+), d) lithium-ion desolvation time, and e) relative EC concentration per mol in the solvation shell versus bulk EC concentration at 20°C for five different electrolyte mixtures calculated using the Advanced Electrolyte Model (AEM). All electrolytes contain 0.4 M $LiPF_6$ and the solvents ratios are by mass.

To further investigate the effect of these different electrolytes on graphite exfoliation, thickness measurements of the encased jelly roll were measured after degassing the

cells by cutting the seal and resealing the cells in a glovebox.[54] Figure 6 shows the result of these experiments. More specifically, Figure 6. a) shows the normalized thickness change, with respect to the initial thickness before the first charging, after formation at C/20 to 3.4 V, while Figure 6. b) shows the thickness change after full formation at C/20 to 4.3 V followed by a discharge to 3.8 V. It is surprising and interesting that the thickness of those cells correlates with the EMC or nitrile reduction rate shown before. For example, the nonlinearity of 2% VC + 1% DTD-based electrolytes is captured in the thickness increase in Figure 6. b). Furthermore, the thickness increase is also observed to be larger when the formation is done at low temperatures and low salt concentrations for electrolytes without additives. It is also observed that the EMC-based electrolyte has a larger thickness increase than the DMC-based electrolyte at 20°C and 3.4 V. Those results suggest that the EMC or nitriles reduction rate is correlated with exfoliation and expansion of the graphite. As a comparison, thickness measurements were also measured for cells containing 1.2 M $LiPF_6$ PC:EMC 3:7 that were charged at 20°C to 4.3 V and then discharged to 3.8 V, where PC corresponds to propylene carbonate. Results show a 1.31 ± 0.06 normalized thickness increase after degassing those cells, which is 7 times as much as cells containing 1.2 M $LiPF_6$ EC:EMC 3:7 that were formed at 20°C. This shows that thickness measurements are able to measure graphite exfoliation since PC is well known to cause the exfoliation of graphite in lithium-ion cells.[54,68,69] This also shows that even if the EC:EMC 3:7 electrolytes result in graphite exfoliation, they are drastically less detrimental than PC:EMC 3:7 electrolytes when the cells containing those electrolytes are formed at 20°C and low salt concentration.

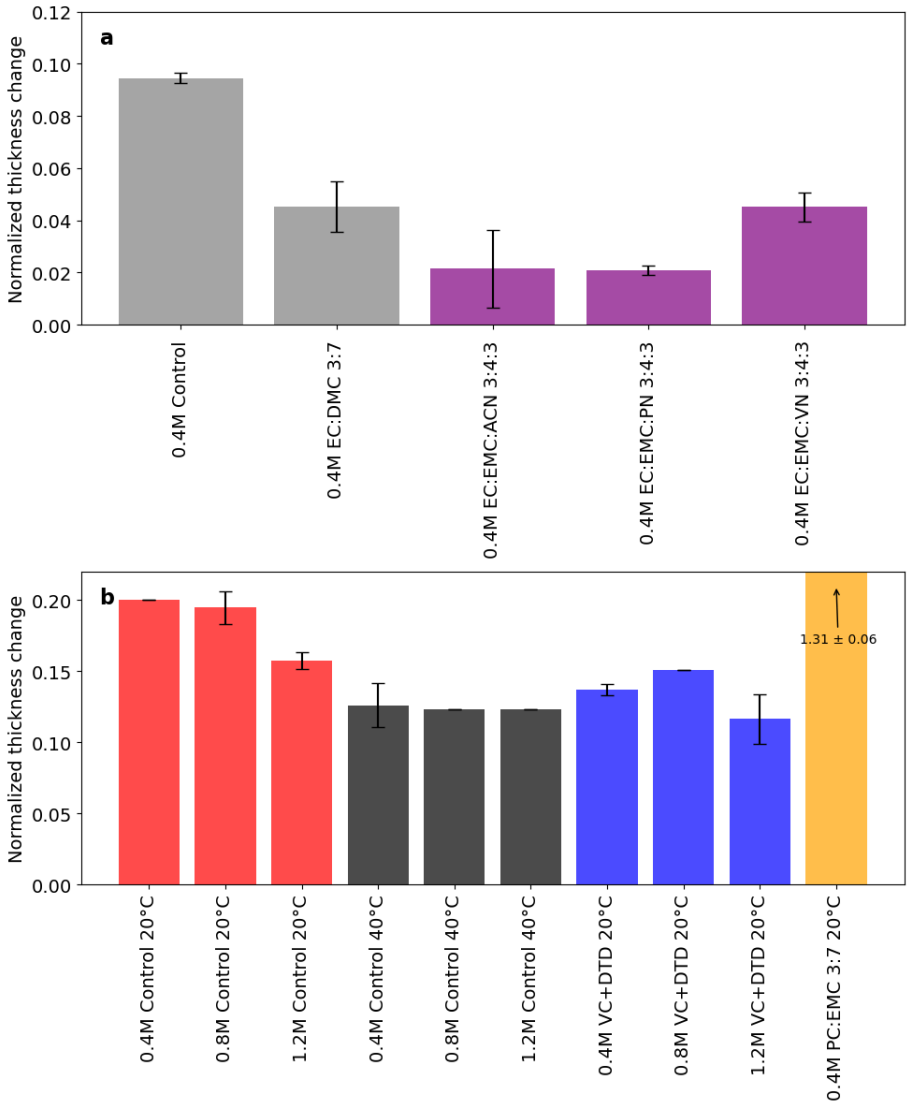

Figure 6: Normalized thickness increases of the encased jelly roll, with respect to the thickness before the first charge, for cells that were formed at 20°C or 40°C. Cells related to the data shown in Subfigure a) were charged to only 3.4 V at 20°C before

measurement, while the data shown in Subfigure b) correspond to cells that were charged to 4.3 V, then discharged to 3.8 V. Cells were charged at a constant C-rate of C/20. The x-axis label uses an abbreviation system. In this abbreviation system, “0.4M Control 20°C” means 0.4 M $LiPF_6$ EC:EMC 3:7 charged at 20°C and “0.8M VC+DTD 20°C” means 0.8 M $LiPF_6$ EC:EMC 3:7 2% VC + 1% DTD charged at 20°C.

To study if the degree of passivation at 20°C and 0.4 M of salt concentration can predict the long-term cycling performance of cells with the same electrolyte at 1.2 M $LiPF_6$, some electrolytes from Figure 3c were selected for cycling. Poor graphite passivation is linked to the growth of the solid electrolyte interphase (SEI), which results in lithium inventory loss. Knowing that SEI growth accelerates at high temperatures, cycling at 55°C and C/2 was undertaken. Figure 7a shows the result of this long-term cycling as discharge capacity versus cycle number for cells containing 1.2 M $LiPF_6$ EC:EMC 3:7 + 2% VC + 1% DTD (in green), 1.2 M $LiPF_6$ EC:EMC 3:7 + 2% VC (in blue), and 1.2 M $LiPF_6$ FEC:EMC 3:7 (in red). Figure 7b also shows ΔV versus cycle number for the same cells, where ΔV corresponds to the average charge voltage minus the average discharge voltage for a specific cycle number.

From the data presented in Figure 7a, it can be observed that the cell with 1.2 M $LiPF_6$ EC:EMC 3:7 + 2% VC + 1% DTD (green) has the highest initial discharge capacities. In contrast, the cells with 1.2 M $LiPF_6$ EC:EMC 3:7 + 2% VC (blue) and 1.2 M $LiPF_6$ FEC:EMC 3:7 (red) show lower initial discharge capacities. From Figure 7b, this difference doesn’t seem to be caused by a different initial growth in ΔV, suggesting

lithium inventory loss due to initial SEI growth. However, these cells recover within the first 50 cycles, and after 100 cycles, all cells exhibit similar capacities, differing by no more than 10 mAh for the C/2 cycles. This can be due to overhang/overlap diffusion effects,[70] SEI dissolution, or active material reactivation. It is worth noting that since those electrolytes are cycling in polycrystalline NMC622/graphite cells at 55°C and C/2, the cycling performance of the 2% VC + 1% DTD-based electrolyte would be drastically different from the performance of past studies.[4,71] In fact, while 2% VC + 1% DTD-based cells can cycle for ~1000 cycles to 95% capacity retention at 40°C and C/3 when the cathode and anode are single crystal NMC532 and graphite, this value decreases to ~250 cycles at 55°C and C/3 for the same electrodes and electrolyte.[4] Using values from a previous study for 2% VC-based electrolyte as an approximation,[56] this value would further decrease for polycrystalline NMC622/graphite cells by roughly four, resulting in an approximation of ~60 cycles to 95% capacity retention for 2% VC + 1% DTD based cells at 55°C and C/3 in NMC622/graphite. In the current study, the cells with 2% VC + 1% DTD achieve 95% capacity retention after 30 cycles when cycled at a higher C-rate of C/2. Furthermore, all cells exhibit signs of overlap/overhang diffusion effects during the first 20 cycles.[70] Therefore, our data aligns well with previous studies.[4,56,71]

The capacity and the ΔV values both reveal an interesting story regarding cell degradation. Figure 7a shows that the capacity loss after 600 cycles is worse for 1.2 M $LiPF_6$ EC:EMC 3:7 2% VC and best for 1.2 M $LiPF_6$ FEC:EMC 3:7, while 1.2 M $LiPF_6$ EC:EMC 3:7 2% VC + 1% DTD shows a medium performance. Figure 7b shows that the rate of impedance growth is fastest for the cell with 1.2 M $LiPF_6$ EC:EMC 3:7 2%

VC. Meanwhile, the cell with 1.2 M $LiPF_6$ EC:EMC 3:7 2% VC + 1% DTD exhibits a slower increase in impedance, which is still slightly faster than the cell containing 1.2 M $LiPF_6$ FEC:EMC 3:7. Interestingly, those trends directly follow the passivation trend observed in Figure 3c. Similarly, the capacity retention trend at 40°C and C/3 from previous studies (see digitized data from some of those studies in Figure S3 and S4) also follows the trend from Figure 3c.[4,56,58,72] While this does not prove direct causation, we hope this will encourage further research in this field.

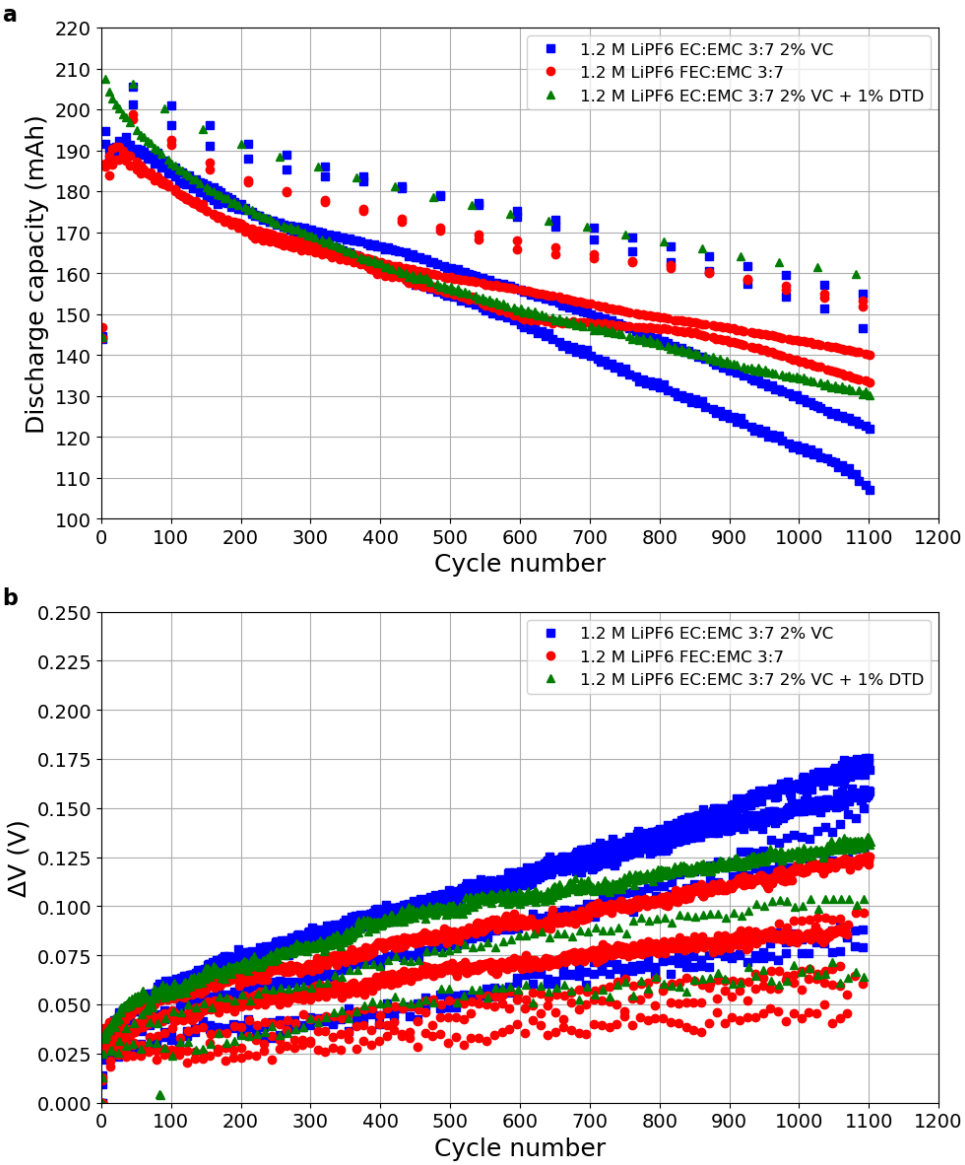

Figure 7: (a) Discharge capacity versus cycle number for cells containing 1.2 M $LiPF_6$ EC:EMC 3:7 + 2% VC + 1% DTD (green triangles), 1.2 M $LiPF_6$ EC:EMC 3:7 + 2% VC (blue squares), and 1.2 M $LiPF_6$ FEC:EMC 3:7 (red circles) at 55°C and C/2 cycling. C/10 checkup cycles were also performed every 50 cycles. (b) ΔV versus cycle number for the same cells, where ΔV corresponds to the average charge voltage minus the average discharge voltage.

Conclusion

By systematically varying the salt concentration, electrolyte composition, and formation temperature, this study provides new insights into the formation and properties of the solid electrolyte interface in lithium-ion batteries. Our investigation reveals that low salt concentrations and low formation temperatures decrease the passivation of the SEI, allowing a rapid performance comparison of different electrolyte formulations by looking at the rate of reduction of linear carbonates. For example, using this method, we reveal that the low-viscosity electrolytes studied here resulted in improved anode passivation due to reduced graphite exfoliation in electrolytes. In addition, this method showed improved passivation for electrolytes containing fluoroethylene carbonate or containing both vinylene carbonate and ethylene sulfate, in agreement with long-term cycling tests. The present work could pave the way for high-throughput studies of new electrolyte formulations.

Acknowledgments

The authors acknowledge the financial support of the Toyota Research Institute for this work.

Reference

1. Ziegler, M. S. & Trancik, J. E. Re-examining rates of lithium-ion battery technology improvement and cost decline. *Energy Environ. Sci.* **14**, 1635–1651 (2021).
2. Investment in lithium-ion batteries could deliver 5.9 TWh capacity by 2030. https://www.spglobal.com/marketintelligence/en/news-insights/research/investment-in-lithium-ion-batteries-could-deliver-5-point-9-twh-capacity-by-2030.
3. Aurbach, D. *et al.* On the use of vinylene carbonate (VC) as an additive to electrolyte solutions for Li-ion batteries. *Electrochimica Acta* **47**, 1423–1439 (2002).
4. Harlow, J. E. *et al.* A Wide Range of Testing Results on an Excellent Lithium-Ion Cell Chemistry to be used as Benchmarks for New Battery Technologies. *J. Electrochem. Soc.* **166**, A3031–A3044 (2019).
5. Madec, L. *et al.* Effect of Sulfate Electrolyte Additives on LiNi1/3Mn1/3Co1/3O2/Graphite Pouch Cell Lifetime: Correlation between XPS Surface Studies and Electrochemical Test Results. *J. Phys. Chem. C* **118**, 29608–29622 (2014).
6. Zhang, L. *et al.* Research on the synergistic effect of fluoroethylene carbonate and lithium difluoro(oxalato)borate in electrolyte on LiNi0.5Mn1.5O4-based high-voltage lithium-ion batteries. *J Mater Sci: Mater Electron* **35**, 524 (2024).
7. Weber, R. *et al.* Long cycle life and dendrite-free lithium morphology in anode-free lithium pouch cells enabled by a dual-salt liquid electrolyte. *Nat Energy* **4**, 683–689 (2019).
8. Xu, M. *et al.* Investigation and application of lithium difluoro(oxalate)borate (LiDFOB) as additive to improve the thermal stability of electrolyte for lithium-ion batteries. *Journal of Power Sources* **196**, 6794–6801 (2011).
9. Michan, A. L. *et al.* Fluoroethylene Carbonate and Vinylene Carbonate Reduction: Understanding Lithium-Ion Battery Electrolyte Additives and Solid Electrolyte Interphase Formation. *Chem. Mater.* **28**, 8149–8159 (2016).
10. Hall, D. S. *et al.* The Solid-Electrolyte Interphase Formation Reactions of Ethylene

Sulfate and Its Synergistic Chemistry with Prop-1-ene-1,3-Sultone in Lithium-Ion Cells. *J. Electrochem. Soc.* **164**, A3445–A3453 (2017).

11. Li, J., Zhao, S., Miah, M. S. & Niu, M. Remaining useful life prediction of lithium-ion batteries via an EIS based deep learning approach. *Energy Reports* **10**, 3629–3638 (2023).
12. Ma, X. *et al.* Editors' Choice—Hindering Rollover Failure of Li[Ni0.5Mn0.3Co0.2]O2/Graphite Pouch Cells during Long-Term Cycling. *J. Electrochem. Soc.* **166**, A711–A724 (2019).
13. Logan, E. R. *et al.* Ester-Based Electrolytes for Fast Charging of Energy Dense Lithium-Ion Batteries. *J. Phys. Chem. C* **124**, 12269–12280 (2020).
14. Logan, E. R. *et al.* A Study of the Transport Properties of Ethylene Carbonate-Free Li Electrolytes. *J. Electrochem. Soc.* **165**, A705–A716 (2018).
15. Gauthier, R. *et al.* How do Depth of Discharge, C-rate and Calendar Age Affect Capacity Retention, Impedance Growth, the Electrodes, and the Electrolyte in Li-Ion Cells? *J. Electrochem. Soc.* **169**, 020518 (2022).
16. Eldesoky, A. *et al.* Long-Term Study on the Impact of Depth of Discharge, C-Rate, Voltage, and Temperature on the Lifetime of Single-Crystal NMC811/Artificial Graphite Pouch Cells. *J. Electrochem. Soc.* **169**, 100531 (2022).
17. Bond, T., Gauthier, R., Eldesoky, A., Harlow, J. & Dahn, J. R. In Situ Imaging of Electrode Thickness Growth and Electrolyte Depletion in Single-Crystal vs Polycrystalline LiNixMnyCozO2/Graphite Pouch Cells using Multi-Scale Computed Tomography. *J. Electrochem. Soc.* **169**, 020501 (2022).
18. Bond, T., Gauthier, R., Gasilov, S. & Dahn, J. R. In-Situ Computed Tomography of Particle Microcracking and Electrode Damage in Cycled NMC622/Graphite Pouch Cell Batteries. *J. Electrochem. Soc.* **169**, 080531 (2022).
19. Aiken, C. P. *et al.* An Apparatus for the Study of In Situ Gas Evolution in Li-Ion Pouch Cells. *J. Electrochem. Soc.* **161**, A1548–A1554 (2014).

20. Sinha, N. N. *et al.* The Use of Elevated Temperature Storage Experiments to Learn about Parasitic Reactions in Wound LiCoO2/Graphite Cells. *J. Electrochem. Soc.* **158**, A1194–A1201 (2011).

21. Steinrück, H.-G. Modeling cyclic voltammetry during solid electrolyte interphase formation: Baseline scenario of a dynamically evolving tunneling barrier resulting from a homogeneous single-phase insulating film. *The Journal of Chemical Physics* **154**, 174703 (2021).

22. Rinkel, B. L. D., Hall, D. S., Temprano, I. & Grey, C. P. Electrolyte Oxidation Pathways in Lithium-Ion Batteries. *J. Am. Chem. Soc.* **142**, 15058–15074 (2020).

23. Han, B. *et al.* Poor Stability of Li2CO3 in the Solid Electrolyte Interphase of a Lithium-Metal Anode Revealed by Cryo-Electron Microscopy. *Advanced Materials* **33**, 2100404 (2021).

24. Morales-Ugarte, J. E. *et al.* EIS and XPS Investigation on SEI Layer Formation during First Discharge on Graphite Electrode with a Vinylene Carbonate Doped Imidazolium Based Ionic Liquid Electrolyte. *J. Phys. Chem. C* **122**, 18223–18230 (2018).

25. Ma, X. *et al.* 1,2,6-Oxadithiane 2,2,6,6-tetraoxide as an Advanced Electrolyte Additive for Li[Ni0.5Mn0.3Co0.2]O2/Graphite Pouch Cells. *J. Electrochem. Soc.* **166**, A2665–A2672 (2019).

26. Spotte-Smith, E. W. C. *et al.* Toward a Mechanistic Model of Solid–Electrolyte Interphase Formation and Evolution in Lithium-Ion Batteries. *ACS Energy Lett.* **7**, 1446–1453 (2022).

27. Wang, Y., Nakamura, S., Ue, M. & Balbuena, P. B. Theoretical Studies To Understand Surface Chemistry on Carbon Anodes for Lithium-Ion Batteries: Reduction Mechanisms of Ethylene Carbonate. *J. Am. Chem. Soc.* **123**, 11708–11718 (2001).

28. An, S. J. *et al.* The state of understanding of the lithium-ion-battery graphite solid electrolyte interphase (SEI) and its relationship to formation cycling. *Carbon* **105**, 52–76 (2016).

29. Zhuang, G. V., Xu, K., Yang, H., Jow, T. R. & Ross, P. N. Lithium Ethylene Dicarbonate Identified as the Primary Product of Chemical and Electrochemical Reduction of EC in 1.2 M LiPF6/EC:EMC Electrolyte. *J. Phys. Chem. B* **109**, 17567–17573 (2005).

30. Wang, L. *et al.* Identifying the components of the solid–electrolyte interphase in Li-ion batteries. *Nat. Chem.* **11**, 789–796 (2019).

31. Vollmer, J. M., Curtiss, L. A., Vissers, D. R. & Amine, K. Reduction Mechanisms of Ethylene, Propylene, and Vinylethylene Carbonates: A Quantum Chemical Study. *J. Electrochem. Soc.* **151**, A178 (2003).

32. Metzger, M., Strehle, B., Solchenbach, S. & Gasteiger, H. A. Hydrolysis of Ethylene Carbonate with Water and Hydroxide under Battery Operating Conditions. *J. Electrochem. Soc.* **163**, A1219 (2016).

33. Bi, Y. *et al.* Stability of Li2CO3 in cathode of lithium ion battery and its influence on electrochemical performance. *RSC Adv.* **6**, 19233–19237 (2016).

34. Nie, M. *et al.* Role of Solution Structure in Solid Electrolyte Interphase Formation on Graphite with LiPF6 in Propylene Carbonate. *J. Phys. Chem. C* **117**, 25381–25389 (2013).

35. Liu, X.-R., Wang, L., Wan, L.-J. & Wang, D. In Situ Observation of Electrolyte-Concentration-Dependent Solid Electrolyte Interphase on Graphite in Dimethyl Sulfoxide. *ACS Appl. Mater. Interfaces* **7**, 9573–9580 (2015).

36. Giffin, G. A. The role of concentration in electrolyte solutions for non-aqueous lithium-based batteries. *Nat Commun* **13**, 5250 (2022).

37. Lin, Y. *et al.* Ultra-stable Li||LiFePO4 batteries via advanced designing of localized high concentration electrolyte. *Journal of Colloid and Interface Science* **628**, 14–23 (2022).

38. Fan, X. *et al.* Highly Fluorinated Interphases Enable High-Voltage Li-Metal Batteries. *Chem* **4**, 174–185 (2018).

39. Zhang, X. *et al.* Unravelling high-temperature stability of lithium-ion battery with lithium-rich oxide cathode in localized high-concentration electrolyte. *Journal of Power*

Sources Advances **5**, 100024 (2020).

40. Bhattacharya, S., Riahi, A. R. & Alpas, A. T. Thermal cycling induced capacity enhancement of graphite anodes in lithium-ion cells. *Carbon* **67**, 592–606 (2014).

41. Aiken, C. P. *et al.* Accelerated Failure in Li[Ni0.5Mn0.3Co0.2]O2/Graphite Pouch Cells Due to Low LiPF6 Concentration and Extended Time at High Voltage. *J. Electrochem. Soc.* **167**, 130541 (2020).

42. Atlung, S., West, K. & Jacobsen, T. Dynamic Aspects of Solid Solution Cathodes for Electrochemical Power Sources. *J. Electrochem. Soc.* **126**, 1311 (1979).

43. Song, W. *et al.* Lithium Difluoro(dioxalato) Phosphate as an Electrolyte Additive for NMC811/Graphite Li-ion Pouch Cells. *J. Electrochem. Soc.* **169**, 110513 (2022).

44. Frisch, M. J. *et al.* Gaussian 16, Revision C.01. Gaussian, Inc. (2016).

45. Becke, A. D. Density-functional thermochemistry. III. The role of exact exchange. *J. Chem. Phys.* **98**, 5648–5652 (1993).

46. Lee, C., Yang, W. & Parr, R. G. Development of the Colle-Salvetti correlation-energy formula into a functional of the electron density. *Phys. Rev. B* **37**, 785–789 (1988).

47. Stephens, P. J., Devlin, F. J., Chabalowski, C. F. & Frisch, M. J. Ab Initio Calculation of Vibrational Absorption and Circular Dichroism Spectra Using Density Functional Force Fields. *J. Phys. Chem.* **98**, 11623–11627 (1994).

48. Tomasi, J., Mennucci, B. & Cammi, R. Quantum Mechanical Continuum Solvation Models. *Chem. Rev.* **105**, 2999–3094 (2005).

49. Hall, D. S., Self, J. & Dahn, J. R. Dielectric Constants for Quantum Chemistry and Li-Ion Batteries: Solvent Blends of Ethylene Carbonate and Ethyl Methyl Carbonate. *The Journal of Physical Chemistry C* **119**, 22322–22330 (2015).

50. Self, J., Hall, D. S., Madec, L. & Dahn, J. R. The role of prop-1-ene-1,3-sultone as an additive in lithium-ion cells. *Journal of Power Sources* **298**, 369–378 (2015).

51. Xiong, D. J., Hynes, T. & Dahn, J. R. Dramatic Effects of Low Salt Concentrations on

Li-Ion Cells Containing EC-Free Electrolytes. *J. Electrochem. Soc.* **164**, A2089 (2017).

52. Ma, L. *et al.* A Guide to Ethylene Carbonate-Free Electrolyte Making for Li-Ion Cells. *J. Electrochem. Soc.* **164**, A5008–A5018 (2017).

53. Gauthier, R., Hall, D. S., Taskovic, T. & Dahn, J. R. A Joint DFT and Experimental Study of an Imidazolidinone Additive in Lithium-Ion Cells. *J. Electrochem. Soc.* **166**, A3707–A3715 (2019).

54. Zhang, N., Eldesoky, A., Dressler, R. A. & Dahn, J. R. Surprising Dependence of the Exfoliation of Graphite During Formation on Electrolyte Composition. *J. Electrochem. Soc.* **170**, 070517 (2023).

55. Thompson, L. M. *et al.* Study of Electrolyte and Electrode Composition Changes vs Time in Aged Li-Ion Cells. *J. Electrochem. Soc.* **168**, 020532 (2021).

56. Hall, D. S., Hynes, T. & Dahn, J. R. Dioxazolone and Nitrile Sulfite Electrolyte Additives for Lithium-Ion Cells. *J. Electrochem. Soc.* **165**, A2961–A2967 (2018).

57. Gauthier, R. *et al.* Impact of functionalization and co-additives on dioxazolone electrolyte additives. *J. Electrochem. Soc.* (2020).

58. Hall, D. S., Gauthier, R., Eldesoky, A., Murray, V. S. & Dahn, J. R. New Chemical Insights into the Beneficial Role of Al2O3 Cathode Coatings in Lithium-ion Cells. *ACS Appl. Mater. Interfaces* **11**, 14095–14100 (2019).

59. Su, C.-C. *et al.* Solvation Rule for Solid-Electrolyte Interphase Enabler in Lithium-Metal Batteries. *Angewandte Chemie International Edition* **59**, 18229–18233 (2020).

60. Li, J. *et al.* Methyl Acetate as a Co-Solvent in NMC532/Graphite Cells. *J. Electrochem. Soc.* **165**, A1027 (2018).

61. Hall, D. S. *et al.* Exploring Classes of Co-Solvents for Fast-Charging Lithium-Ion Cells. *J. Electrochem. Soc.* **165**, A2365–A2373 (2018).

62. González, B., Calvar, N., Gómez, E. & Domínguez, Á. Density, dynamic viscosity, and derived properties of binary mixtures of methanol or ethanol with water, ethyl acetate, and

methyl acetate at T = (293.15, 298.15, and 303.15) K. *The Journal of Chemical Thermodynamics* **39**, 1578–1588 (2007).

63. Gravelle, S., Kamal, C. & Botto, L. Liquid exfoliation of multilayer graphene in sheared solvents: A molecular dynamics investigation. *The Journal of Chemical Physics* **152**, 104701 (2020).

64. Fernandes, J., Nemala, S. S., De Bellis, G. & Capasso, A. Green Solvents for the Liquid Phase Exfoliation Production of Graphene: The Promising Case of Cyrene. *Front. Chem.* **10**, (2022).

65. Diasio, M. A. & Green, D. L. The Effect of Solvent Viscosity on Production of Few-layer Graphene from Liquid-phase Exfoliation of Graphite. *MRS Advances* **4**, 241–247 (2019).

66. Rohman, N., Mohiuddin, T. & Al-Ruqeishi, M. S. Surface free energy of graphene-based coatings and its component elements. *Inorganic Chemistry Communications* **153**, 110855 (2023).

67. Wang, Z. *et al.* A nitrile solvent structure induced stable solid electrolyte interphase for wide-temperature lithium-ion batteries. *Chem. Sci.* (2024) doi:10.1039/D4SC03890H.

68. Shi, P. C. *et al.* Effect of propylene carbonate-Li+ solvation structures on graphite exfoliation and its application in Li-ion batteries. *Electrochimica Acta* **247**, 12–18 (2017).

69. Röser, S. *et al.* Highly Effective Solid Electrolyte Interphase-Forming Electrolyte Additive Enabling High Voltage Lithium-Ion Batteries. *Chem. Mater.* **29**, 7733–7739 (2017).

70. Gyenes, B., Stevens, D. A., Chevrier, V. L. & Dahn, J. R. Understanding Anomalous Behavior in Coulombic Efficiency Measurements on Li-Ion Batteries. *J. Electrochem. Soc.* **162**, A278 (2014).

71. Taskovic, T., Eldesoky, A., Song, W., Bauer, M. & Dahn, J. R. High Temperature Testing of NMC/Graphite Cells for Rapid Cell Performance Screening and Studies of Electrolyte Degradation. *J. Electrochem. Soc.* **169**, 040538 (2022).

72. Cha, J., Han, J.-G., Hwang, J., Cho, J. & Choi, N.-S. Mechanisms for electrochemical

performance enhancement by the salt-type electrolyte additive, lithium difluoro(oxalato)borate, in high-voltage lithium-ion batteries. *Journal of Power Sources* **357**, 97–106 (2017).